

Intravoxel incoherent motion diffusion-weighted imaging in the liver: comparison of mono-, bi- and tri-exponential modelling at 3.0-T

Jean-Pierre Cercueil · Jean-Michel Petit · Stéphanie Nougaret · Philippe Soyer ·
Audrey Fohlen · Marie-Ange Pierredon-Foulongne · Valentina Schembri ·
Elisabeth Delhom · Sabine Schmidt · Alban Denys · Serge Aho · Boris Guiu

Received: 10 March 2014 / Revised: 31 October 2014 / Accepted: 3 December 2014 / Published online: 20 December 2014
© European Society of Radiology 2014

Abstract

Purpose To determine whether a mono-, bi- or tri-exponential model best fits the intravoxel incoherent motion (IVIM) diffusion-weighted imaging (DWI) signal of normal livers.

Materials and methods The pilot and validation studies were conducted in 38 and 36 patients with normal livers,

respectively. The DWI sequence was performed using single-shot echoplanar imaging with 11 (pilot study) and 16 (validation study) b values. In each study, data from all patients were used to model the IVIM signal of normal liver.

Diffusion coefficients ($D_i \pm$ standard deviations) and their fractions ($f_i \pm$ standard deviations) were determined from each model. The models were compared using the extra sum-of-squares test and information criteria.

Results The tri-exponential model provided a better fit than both the bi- and mono-exponential models. The tri-exponential IVIM model determined three diffusion compartments: a slow ($D_1 = 1.35 \pm 0.03 \times 10^{-3} \text{ mm}^2/\text{s}$; $f_1 = 72.7 \pm 0.9 \%$), a fast ($D_2 = 26.50 \pm 2.49 \times 10^{-3} \text{ mm}^2/\text{s}$; $f_2 = 13.7 \pm 0.6 \%$) and a very fast ($D_3 = 404.00 \pm 43.7 \times 10^{-3} \text{ mm}^2/\text{s}$; $f_3 = 13.5 \pm 0.8 \%$) diffusion compartment [results from the validation study]. The very fast compartment contributed to the IVIM signal only for b values $\leq 15 \text{ s}/\text{mm}^2$

Conclusion The tri-exponential model provided the best fit for IVIM signal decay in the liver over the 0–800 s/mm^2 range. In IVIM analysis of normal liver, a third very fast (pseudo)diffusion component might be relevant.

Key Points

- For normal liver, tri-exponential IVIM model might be superior to bi-exponential
- A very fast compartment ($D = 404.00 \pm 43.7 \times 10^{-3} \text{ mm}^2/\text{s}$; $f = 13.5 \pm 0.8 \%$) is determined from the tri-exponential model
- The compartment contributes to the IVIM signal only for $b \leq 15 \text{ s}/\text{mm}^2$

J.-P. Cercueil · J.-M. Petit
University of Burgundy, INSERM U866, BP 87900, 21079 Dijon, France

J.-P. Cercueil
Department of Radiology, CHU (University Hospital), BP 77908, 21079 Dijon, France

J.-M. Petit
Department of Endocrinology, Diabetology, and Metabolic Diseases, CHU (University Hospital), BP 77908, 21079 Dijon, France

S. Nougaret · M.-A. Pierredon-Foulongne · V. Schembri ·
E. Delhom · B. Guiu (✉)
Department of Radiology, St-Eloi University Hospital, 34295 Montpellier, France
e-mail: B-guiu@chu-montpellier.fr

P. Soyer
Department of Body and Interventional Imaging, Hôpital 1 Lariboisière, Assistance Publique Hôpitaux de Paris, 75475 Paris Cedex 10, France

A. Fohlen
Department of Radiology, University Hospital, 14011 Caen, France

S. Schmidt · A. Denys
Department of Radiology, Centre Hospitalier Universitaire Vaudois, Lausanne, Switzerland

S. Aho
Department of Biostatistics, CHU (University Hospital), BP 77908, 21079 Dijon, France

Keywords Diffusion-weighted imaging · IVIM · Liver · Signal model · MRI

Introduction

Intravoxel incoherent motion (IVIM) reflects the random microscopic motion that occurs in voxels on magnetic resonance (MR) images of water molecules (either intra-cellular or extra-cellular) and the microcirculation of blood [1–4]. Initially, it was claimed that signal attenuation as a function of b was mono-exponential in diffusion-weighted imaging (DWI), owing to a mono-compartmental model of water diffusion [1, 3, 5]. However, in 1988, le Bihan et al. [4] proved that it was possible to identify two different compartments of diffusion in the brain. According to IVIM theory, the fast component of diffusion (represented by D^*) is related to microperfusion, whereas the slow component (represented by D) is linked to pure molecular diffusion. Owing to this bi-compartmental model, the signal decay of IVIM DWI was described using a bi-exponential model [4]. Though IVIM studies have long been limited to the brain due to technical limitations in moving organs [6], the door has recently opened on applications of IVIM in the liver [2, 7–15].

Interestingly, the liver is anatomically and physiologically different from the brain, and may be more complex. These differences include the presence of several vessel types (arteries/arterioles, portal veins/venules, hepatic veins/venules), sinusoid capillaries, bile ducts, a rich lymphatic system [16], and a functionally important intermediate area between the sinusoids and hepatocytes, called the space of Disse [16]. Flowing or moving spins are present in these compartments, which are directly or indirectly connected together. This could support the hypothesis that more than two diffusion compartments may exist in the liver [17].

However, bi-exponential modelling of the IVIM signal in a single patient or even in single voxels is known to be challenging [2, 9, 10, 12, 18] with a lack of reproducibility especially for D^* calculations, owing to the limited sampling and signal-to-noise ratio (SNR). The increase in the degree of freedom of the IVIM model without both adequate sampling and improved SNR results in fitting failure. It has been proposed to average the data of several patients in order to improve the SNR [8, 19]. In order to keep individual data, the averaging over multiple data points per patient might also improve the data quality.

The aim of this study was to compare mono-, bi- and tri-exponential models without any assumption regarding their diffusion coefficient(s) in order to determine which of them best fits the IVIM signal of normal liver. To avoid drawing erroneous conclusions, we prospectively validated the results in another population of patients using a different IVIM sequence.

Materials and methods

The pilot and the validation studies were approved by our regional ethics committee. Written informed consent was obtained from all patients.

Pilot study

The pilot study included a series of type-2 diabetic patients with a presumed normal liver. Between December 2010 and September 2012, 149 consecutive patients were screened at the endocrinology department of our institution for type 2 diabetes. The inclusion criteria were: an age older than 18-years-old; body weight less than 150 kg; no known acute or chronic disease (other than diabetes) according to the patient's medical history with physical examination and standard laboratory tests; alcohol consumption of less than 20 g per day; and no evidence of liver disease such as viral hepatitis. These patients underwent MRI as outpatients for their annual disease assessment or for educational purposes. Four patients were excluded for claustrophobia.

To ensure that patients enrolled in the pilot study had a normal liver, we excluded patients with $>5\%$ liver steatosis (as evaluated on proton MR spectroscopy [20–22]), those with a liver $T2^*$ lower than 15 msec (as calculated using triple-echo gradient-echo sequences [21, 22]), which reflects hepatic iron overload, and those with a Fibrotest[®] $> F1$ [23–25]. Therefore, the pilot study was conducted in 38 patients (20 women and 18 men) with a mean age of 43.4 years (range: 20–79 years), a mean steatosis of 1.02 % (range: 0.14–4.59 %, SD: 0.9), and a mean $T2^*$ value of 19.95 msec (range: 16–27 msec; SD: 2.7).

MR Imaging

MR imaging was performed with a 3.0 T unit (Magnetom Trio; Siemens Erlangen, Germany) with a peak gradient amplitude of 45 mT/m and a time to peak of 204 μ sec. A six-element body phased-array coil system was used. All patients were carefully instructed to suspend respiration in expiration and to be consistent in their breath-holds. To allow correct positioning, localizing sequences in the coronal, transverse, and sagittal planes were acquired during a breath-hold.

As mentioned above and as previously reported [21, 22], we performed seven proton-MR spectroscopic sequences (for correction of $T2$ decay) for the evaluation of steatosis, and a spoiled triple-echo gradient-echo sequence for $T2^*$ calculation (Appendix 1).

IVIM DW Imaging Sequence

The IVIM DW imaging sequence was performed during the same MR examination and was acquired using navigator-echo triggered PACE (prospective acquisition correction, Siemens Healthcare) single-shot echoplanar imaging (SS EPI) with twice-refocused bipolar diffusion preparation and 11 b values (Table 1).

IVIM DW-MRI analysis

As previously underlined [26, 27], separating microperfusion from pure molecular diffusion requires a high SNR. With the aim to optimize this ratio, we measured the liver signal as follows. At each *b* value, the recorded SI was obtained by averaging the mean SI in a 1 cm-ROI in the right liver (avoiding extra-hepatic fat, large hepatic vessels or bile ducts) positioned by a radiologist (JPC, with 19 years of experience in liver imaging) on three slices. These ROIs were initially positioned on images with *b*=0 s/mm², then copied and pasted on each corresponding image for each *b* value.

Since we aimed to model a (presumed) normal liver, we recorded the signal values at each *b* level after normalization by attributing a value of 100 at *b*=0 s/mm² ($S_{norm}=(SI/SI_0)*100$ where S_{norm} is the normalized signal, SI =signal at a given *b* value, and SI_0 =signal at *b*=0 s/mm²). Using this normalization, the S_{norm} value was independent from the signal value at *b*=0 s/mm², thus, giving the same weight to each patient in order to globally analyse the signal of a normal liver.

If diffusion is considered mono-compartmental, signal attenuation as a function of *b* is expressed using the following mono-exponential equation:

$$SI = SI_0 \cdot e^{-b \cdot ADC}$$

where SI is the signal intensity at the given *b* value, ADC is the apparent diffusion coefficient, and SI_0 is proportional to e^{-TE/T_2} .

According to IVIM theory [1, 2, 4], diffusion is considered bi-compartmental (pseudo-diffusion [also called perfusion-related diffusion] and pure molecular diffusion), which explains why signal attenuation as a function of *b* is expressed by a bi-exponential equation:

$$SI = SI_0 \cdot [f_1 \cdot e^{-b \cdot D_1} + f_2 \cdot e^{-b \cdot D_2}] \tag{1}$$

where f_2 (i.e., perfusion fraction usually called *f*) and f_1 (usually called (1-*f*)) represent the fraction of each diffusion compartment, D_2 (usually called D^*) represents perfusion-related diffusion, and D_1 (usually called D) represents pure molecular diffusion.

If diffusion is considered as tri-compartmental, signal attenuation is expressed by the following tri-exponential equation:

$$SI = SI_0 \cdot [f_1 \cdot e^{-b \cdot D_1} + f_2 \cdot e^{-b \cdot D_2} + f_3 \cdot e^{-b \cdot D_3}]$$

Where $f_1, f_2,$ and f_3 represent the fractions of each diffusion compartment ($f_1 + f_2 + f_3 = 1$) and $D_1, D_2,$ and D_3 represent the diffusion / pseudo-diffusion coefficient of each compartment.

Then to avoid erroneous conclusions, we validated the results in a prospective series of patients.

Validation study

The validation study prospectively included type-1 diabetic patients with a presumed normal liver. Between December 2012 and October 2013, 61 consecutive patients were screened at the endocrinology department of our institution for type 1 diabetes. The inclusion criteria were exactly the same as those used for the pilot study. These patients were imaged as outpatients for annual disease assessment or educational purposes. Two patients were excluded for claustrophobia.

To ensure that patients enrolled in the validation study had a normal liver, patients with >5 % liver steatosis, with a liver T_2^* lower than 15 msec, or with a Fibrotest® > F1 were excluded (as for the pilot study). Therefore, the validation study was conducted in 36 patients with mean age 42 years (range: 19-72 years), 16 women and 20 men, a mean steatosis of 0.72 (range: 0.1-4.33 %, SD: 1), and a T_2^* value of 21.5 msec (range: 16-33 msec; SD: 3.3).

Table 1 IVIM DWI sequence parameters

	PILOT STUDY	VALIDATION STUDY
Acquisition plane	Axial	Axial
TR	1 respiratory cycle	1 respiratory cycle
TE	68 ms	67 ms
<i>b</i> -values (s/mm ²)	0, 5, 15, 25, 35, 50, 100, 200, 400, 600, 800	0, 5, 10, 15, 20, 25, 30, 35, 40, 45, 50, 100, 200, 400, 600, 800
EPI factor	128	128
Field of view (mm)	400	400
Slice thickness/interslice gap (mm)/nb of slices	7.0 / 1.4 / 20	7.0 / 1.4 / 20
Parallel imaging factor	2	2
Scan time (min)	≈5	≈5
Number of averages	3	1
Acquisition matrix	256 x 256	256 x 256

MR imaging was performed on the same MR system. Localizing sequences, MR spectroscopic sequences, and triple-echo gradient-echo sequences were the same as for the pilot study.

Since we aimed to validate a tri-exponential model as independent from the chosen b values, we used more b -values ($n=16$) in combination with less numbers of signal averages keeping acquisition time constant (parameters in Table 1). IVIM MR-DWI data analysis was performed using the same protocol (ROIs, signal normalization) as for the pilot study (Fig. 1).

Statistical analysis

The estimation of diffusion parameters and their standard deviations was carried out using a nonlinear least squares regression model. A robust variance estimator was used to take into account the cluster-correlated data (i.e., several measurements per patient, since data were not averaged) and *heteroscedasticity* (i.e., unequal variances) [28]. Three models were assessed: single-, bi-, and tri-exponential decay. The initial values of diffusion parameters for each model were obtained by “exponential feathering”. A Wald test was used to test the hypothesis that diffusion parameters were different

from zero. The assumption of normality of residuals (part of model adequacy) was checked using tests based on skewness and kurtosis. Models were compared via two strategies: using the extra sum-of-squares test [29] and using information criteria. For the latter strategy, we calculated the Akaike information criterion (AIC), the second-order Akaike information criterion (AICc), delta AIC (instead of AICc because AIC was almost equal to AICc in our study), and relative likelihood as suggested by Anderson [30]. The best fitting exponential model was selected based on the criteria above. All analyses were performed using Stata software version 12 (Stata corporation, College Station, TX, USA). A P -value below .05 was considered significant.

Results

Pilot study

Normalized signal values and the averaged curve for the pilot study are shown in Fig. 2. Diffusion coefficients for mono-, bi-, and tri-exponential models determined from nonlinear regression are reported in Table 2. Using the extra sum-of-squares

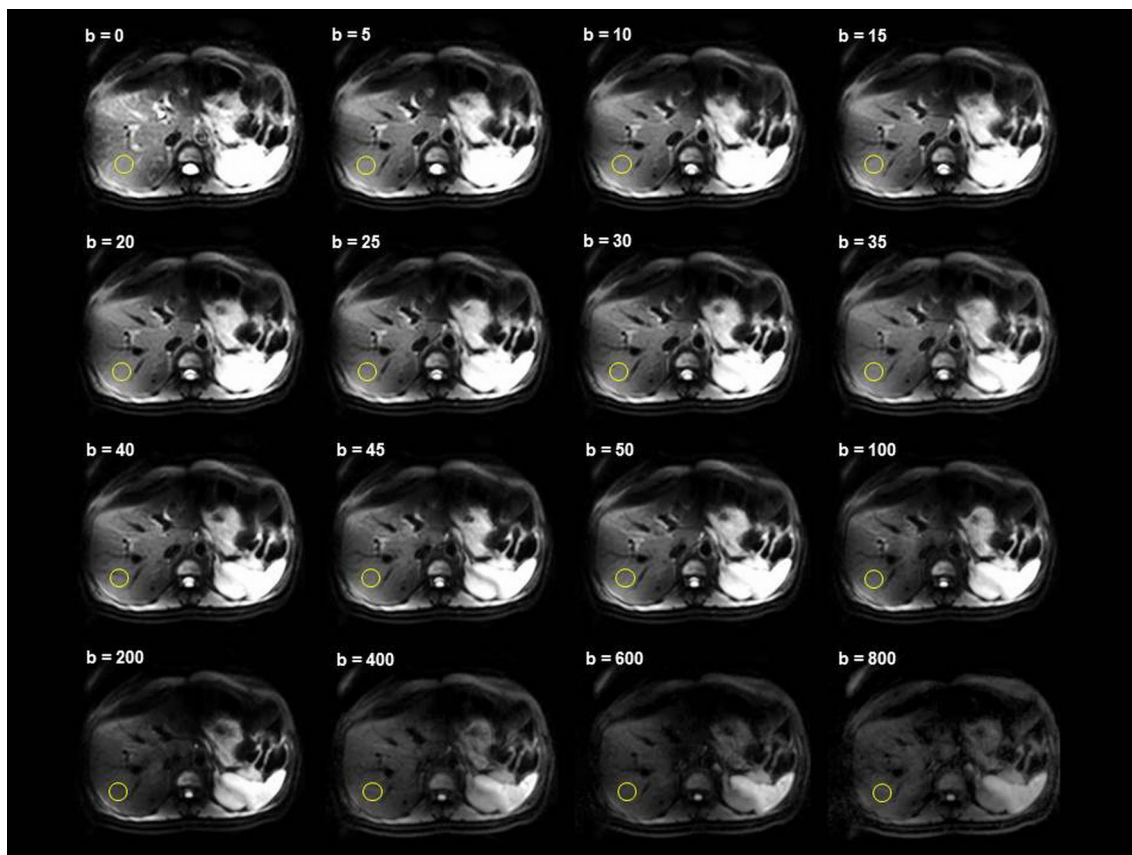


Fig. 1 Axial MR image from the 16 b IVIM DWI sequence used for the validation study. A typical ≈ 1 cm region of interest within the liver parenchyma (avoiding extra-hepatic fat, large hepatic vessels and bile ducts) used for signal measurement is shown

test, the bi-exponential model provided a better fit than the mono-exponential model ($P<.001$) and the tri-exponential model provided a better fit than the bi-exponential model ($P<.001$) (Table 3). Using information criteria, the tri-exponential model provided a better fit than the bi-exponential model, which in turn provided a better fit than the mono-exponential model (Table 4).

Validation study

Diffusion coefficients for each model determined in the validation study are reported in Table 5. Mono-, bi-, and tri-exponential regression curves are shown in Fig. 3. Comparison of the three models using the extra sum-of-squares test (Table 6) and the information criteria (Table 7) showed the same results as for the pilot study. The tri-exponential model provided a better fit than the bi-exponential model, which in turn provided a better fit than the mono-exponential model. The contribution of each diffusion compartment to the total signal is reported in Table 8.

Discussion

We found that a tri-exponential model provided a better fit for DWI signal decay of the normal liver than did the classical bi-exponential model, initially described by Le Bihan [4, 31]. The original IVIM model considered two different compartments: a slow diffusion compartment related to either intra-cellular or extra-cellular pure molecular diffusion (represented

Table 2 Results of the nonlinear regression applied in the pilot study using a mono-, bi-, and tri-exponential model

Model	Variable	Coefficient±SD	P*
Mono-exponential	ADC	$1.80\pm 0.04\cdot 10^{-3}$ mm ² /s	<.001
Bi-exponential	D ₁ (=D)	$1.47\pm 0.03\cdot 10^{-3}$ mm ² /s	<.001
Tri-exponential	f ₁	73.1±1 %	<.001
	D ₂ (=D*)	$125.43\pm 8.39\cdot 10^{-3}$ mm ² /s	<.001
	f ₂ (=f)	25.7±0.9 %	<.001
	D ₁	1.23 ± 0.03 10 ⁻³ mm ² /s	<.001
	f ₁	65.3±1.4 %	<.001
	D ₂	19.54 ± 1.32 10 ⁻³ mm ² /s	<.001
	f ₂	17.6 %±1.5	<.001
D ₃	391.96 ± 39.34 10 ⁻³ mm ² /s	<.001	
f ₃	17.1±1.3 %	<.001	

*Wald test

by D), and a rapid diffusion compartment related to microperfusion (represented by D*). In our study, we demonstrated that a third diffusion compartment could exist. We believe that this finding is not an artefact since 1) we made no specific assumption regarding this third compartment and 2) the results of the pilot study were confirmed in the validation study using a different population of patients, as well as a different number and a different distribution of the *b* values. The precise origin of the third compartment is beyond the scope of this study, but we can make two observations: First, according to IVIM theory [1, 2, 4], the fast component of diffusion is linked to perfusion by the equation $D_{fast} = \frac{l \cdot v}{6}$, where *l* is the mean length of the capillary segment and *v* is the mean velocity of capillary blood. With $a \approx 400 \cdot 10^{-3}$ mm²/s diffusion coefficient, this compartment clearly contains very

Fig. 2 Individual normalized signal values at each *b* value (small squares) and fitting curve (red curve) derived from an averaged data set obtained from all the individual data points at each *b*-value for the pilot study (11 *b* values). Please note that it is only an illustration since our methodology did not average all patient data before fitting, but took into account all individual data for fitting

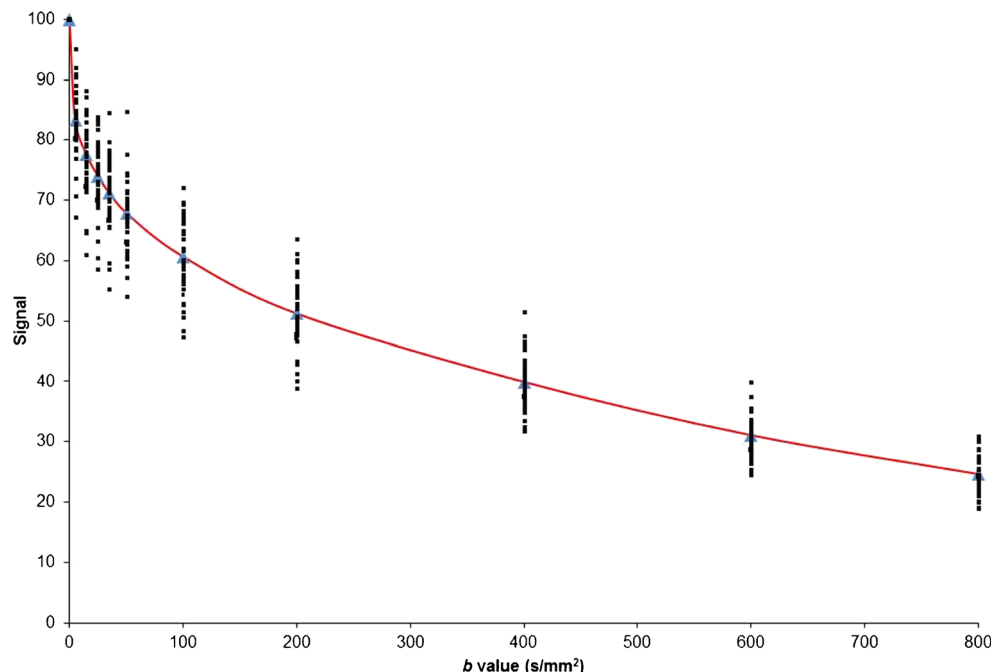


Table 3 Comparison in the pilot study of mono-, bi-, and tri-exponential models using extra sum-of-squares tests (F tests)

Models	Sum of squares	Degrees of freedom	Mean squared error	Relative difference	Relative difference ratio (F)	P
Mono-exponential	32 157.52	416	77.30	Mono- vs. Tri-exponential	203.6	<.001
Bi-exponential	12 495.86	414	30.18	Bi- vs. Tri-exponential	32.3	<.001
Tri-exponential	10 803.91	412	26.22	/	/	/

rapid flowing spins. Second, diffusion is characterized by a diffusion sphere whose radius is defined by $R=(6Dt)^{1/2}$ as the mean squared displacement of a water molecule with diffusion coefficient D from the centre of the sphere in time t . For $D=400\times 10^{-3}$ s/mm² and $t\approx 50$ msec (i.e., diffusion time), the calculated R is ≈ 350 μ m. This radius is considerably larger than the diameter of terminal arterioles (≈ 22 μ m), portal venules (≈ 53 μ m), or hepatic venules (≈ 33 μ m) in the hepatic lobule [32]. Thus, flowing spins of the third compartment are probably located in larger vessels (arterioles and/or portal venules and/or hepatic venules), which exhibit IVIM characteristics as long as they are randomly oriented and so numerous that the spins lose their phase memory during the measurement period [33]. The second compartment with a diffusion coefficient ($\approx 25\times 10^{-3}$ mm²/s) that is ten times greater than the diffusion coefficient of free water (2.5×10^{-3} mm²/s at 40 °C) probably reflects microperfusion effects. Such an admixture of various perfusion components in liver parenchyma has already been proposed and referred to as the multiple-perfusion-components theory [17].

Interestingly, according to the literature regarding bi-exponential IVIM DWI of the normal liver, there is a tendency for D^* to increase when the number of very low (<20 s/mm²) b values increases. For one very low b value (i.e., $b=0$ s/mm²), D^* was reported as being between $27\text{--}52\times 10^{-3}$ mm²/s [7, 9, 11, 14, 15] while it was between $60\text{--}100\times 10^{-3}$ mm²/s for two very low b values [8, 10], and between $75\text{--}110\times 10^{-3}$ mm²/s for three very low b values [2, 6, 12, 13]. The D^* value in our series (121×10^{-3} mm²/s), calculated using four very low b values, is in keeping with these results. Interestingly, in the study by Delattre et al. [8], D^* of the liver was calculated from the same acquisition (13 b IVIM sequence) using either 13 b values ($D^*=100.3\times 10^{-3}$ mm²/s from $b=0, 15, 30, 45, 60, 75, 90, 105, 120, 250, 350, 450, 550$ s/mm²) or only 9 b values

Table 4 Comparison in the pilot study of mono-, bi-, and tri-exponential models using information criteria

Models	AIC	AICc	Delta AIC	Relative likelihood
Mono-exponential	3005.57	3005.60	223.96	5.42×10^{-98}
Bi-exponential	2614.46	2614.56	28.41	4.6×10^{-13}
Tri-exponential	2557.64	2557.85	0	1

AIC indicates Akaike Information Criterion

AICc indicates second-order Akaike Information Criterion

($D^*=75.6\times 10^{-3}$ mm²/s from $b=0, 30, 60, 75, 90, 120, 250, 450, 550$ s/mm²). Again, the use of an additional very low b value ($b=15$ s/mm²) resulted in a greater D^* , whereas D did not differ (1.53×10^{-3} mm²/s using 13 b versus 1.54×10^{-3} mm²/s using 9 b values). This tendency for D^* to increase when the number of very low b values increases reflects the contamination of perfusion-related diffusion (derived from the standard bi-exponential IVIM model) by the third compartment, which contributes to the IVIM signal only for b values within the 0–15 s/mm² range (Table 8).

Hayashi et al., published two papers in which they used a tri-exponential model to fit the diffusion signal in cirrhosis [11] and steatosis [34]. Since they used higher b values (i.e., until 1500s/mm²) and did not sample the diffusion signal decay in the 0–50s/mm² range, they reported two diffusion components instead of two perfusion components like in our study. Thus, it is not unlikely that four diffusion compartments (or more) may exist in the liver.

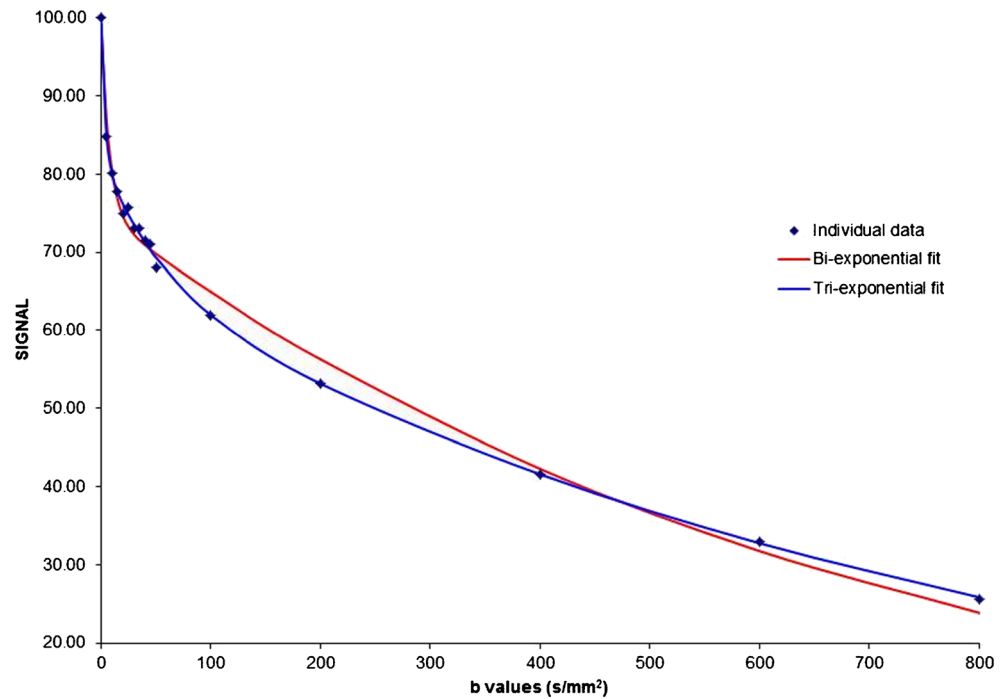
The principle of averaging several ROI measurements per patient [35, 36], which are in turn averaged for all patients to model the IVIM signal, has been already used to improve the SNR ratio [8, 19]. Our derived methodology may explain why we report much lower SDs for diffusion coefficients than those usually reported in the literature. Yet, these SDs still remained high for the two fastest diffusion compartments. It has been reported that an increased number of b values (i.e., sampling) results in a more precise estimation of the diffusion coefficients [2, 9, 10, 12, 18]. However, to keep within an acceptable acquisition time, we had to reduce the number of

Table 5 Results of the nonlinear regression applied in the validation study using a mono-, bi-, and tri-exponential model

Model	Variable	Coefficient \pm SD	P*
Mono-exponential	ADC	1.72 ± 0.04 10^{-3} mm ² /s	<.001
Bi-exponential	D_1 (=D)	1.50 ± 0.03 10^{-3} mm ² /s	<.001
Tri-exponential	f_1	77 ± 0.4 %	<.001
	D_2 (=D*)	121 ± 9.64 10^{-3} mm ² /s	<.001
	f_2 (=f)	21 ± 0.7 %	<.001
	D_1	1.35 ± 0.03 10^{-3} mm ² /s	<.001
	f_1	72.7 ± 0.9 %	<.001
	D_2	26.50 ± 2.49 10^{-3} mm ² /s	<.001
	f_2	13.7 ± 0.6 %	<.001
	D_3	404.00 ± 43.70 10^{-3} mm ² /s	<.001
	f_3	13.5 ± 0.8 %	<.001

*Wald test

Fig. 3 Bi- (red curve) and tri-exponential (blue curve) modelling of the averaged IVIM signal obtained from one patient of the validation study (16 *b* values). This illustrates that tri-exponential modelling provided a better fit to the IVIM signal



signal acquisitions (only one for the 16 *b* sequence). Despite the use of state-of-the-art gradient hardware, 3 T acquisition, respiratory triggering, parallel imaging, and reduced TE, the SNR still remained low for IVIM DWI of the liver. This is a major cause of difficulties in modelling the fast compartment(s) of diffusion. We notice in Table 8 that for $b=0$ s/mm², each of the first two compartments contributed to only 13 % of the total signal. This proportion falls very quickly when *b* values increase. If noise is considered constant, the SNR from the two fastest diffusion compartments at $b=0$ is half that of the global IVIM signal at $b=800$ s/mm². This very low SNR can at least partly explain why the reliable and precise determination of corresponding diffusion coefficients is extremely challenging.

As mentioned above, the quality of sampling (i.e., the number of *b* values used) is also a critical point to precisely estimate these coefficients. In our validation study using 16 *b* values, only the first compartment (S1 signal) contributed to the IVIM signal over the 200–800 s/mm² range. Over the 15–150 s/mm² range (9 *b* values), both the first and second compartment contributed to the IVIM signal while over the 0–10s/mm² range (3 *b* values), the three compartments

contributed. Therefore, for the third compartment, we have both a low SNR and very low sampling. It was, thus, logical for measurement to be imprecise. For the second compartment, we were able to achieve an adequate number of samples (9 *b* values in the 15–100 s/mm² range), but as for *D** estimation in the bi-exponential IVIM model, the SNR still has to be improved to obtain reliable and precise results. New IVIM sequences that allow a flexible number of acquisitions for each *b* value in clinically acceptable acquisition times, when available, should at least partly compensate for the low SNR.

The pooled analysis from different patients with a normal liver was useful to demonstrate the existence of a third compartment, but in clinical practice, the aim is to calculate diffusion parameters at an individual level. For bi-exponential IVIM, a segmented approach, that is to say calculating *D* then *f* then *D**, has frequently been used in the literature [2, 11, 13–15] since simultaneous fitting of all diffusion parameters usually gives unstable results. By using only *b* values >15 s/mm², the tri-exponential model can be reduced to a bi-exponential model since the third compartment no longer contributes to the IVIM signal. Then, a segmented approach may be used to model the first and second

Table 6 Comparison in the validation study of mono-, bi-, and tri-exponential models using extra sum-of-squares tests (F tests)

Models	Sum of squares	Degrees of freedom	Mean squared error	Relative difference	Relative difference ratio (F)	<i>P</i>
Mono-exponential	25 440.29	574	44.32	Mono- vs. Tri-exponential	238.98	<.001
Bi-exponential	10 460.97	572	18.29	Bi- vs. Tri-exponential	28.73	<.001
Tri-exponential	9 502.98	570	16.67	/	/	/

Table 7 Comparison in the validation study of mono-, bi-, and tri-exponential models using information criteria

Models	AIC	AICc	Delta AIC	Relative likelihood
Mono-exponential	3820.49	3820.52	279.60	$3,72^{\circ}10^{-122}$
Bi-exponential	3312.61	3312.68	25.66	$7,17^{\circ}10^{-12}$
Tri-exponential	3261.29	3261.44	0	1

AIC indicates Akaike Information Criterion

AICc indicates second-order Akaike Information Criterion

compartment. The acquisition of only $>15 \text{ s/mm}^2$ b values would give the opportunity to simplify the tri-exponential model and to increase the number of samples to model the first two compartments. This approach needs to be explored in a future work.

Several limitations of this study must be acknowledged. First, we selected patients with a presumed normal liver, without histological confirmation. However, since liver biopsy in this context was not ethically acceptable, we combined multiple criteria (based on patients’ history, clinical examinations, biological markers, the Fibrotest[®], and the absence of liver steatosis or iron overload as determined by multimodal MRI) to rule out liver disease. Second, the liver and blood have completely different T2 times [2] and f values are strongly influenced by these different T2 times. We did not calculate T2-corrected f values [19], since we could not make sure that

the second and third compartment of diffusion corresponded to blood. The use of different TEs between the pilot and the validation study would have allowed us to calculate the differences between the T2 relaxation times of the second and third compartments [6, 19], and would, thus, have indicated whether or not they had the same nature (blood). However, since we aimed to minimize the TE to improve the SNR in this study, TEs were almost similar. Third, we did not consider noise (especially Rician noise) influence in the diffusion signal decay. However, its influence was probably limited since we used relatively low b values ($\leq 800 \text{ s/mm}^2$) with the aim to preserve a high SNR. Fourth, our study was designed for the normal liver. The behaviour of the IVIM signal could be different in tumours or maybe in diffuse liver diseases like cirrhosis or steatosis. The adequacy of the tri-exponential model in these settings needs to be explored in further studies. Finally, we did not assess other multi-compartmental models (four compartments or more) given the technical limitations regarding sampling and the SNR of our IVIM sequences.

In conclusion, the tri-exponential model provides a better fit for IVIM signal decay in the liver than the classical bi-exponential model across the 0-800 s/mm^2 range. The tri-exponential model accounts for three different compartments: a slow component of diffusion corresponding to classical pure molecular diffusion, a fast diffusion compartment with $a \approx 20 \times 10^{-3} \text{ mm}^2/\text{s}$ diffusion coefficient, and a very fast diffusion compartment with $a \approx 400 \times 10^{-3} \text{ mm}^2/\text{s}$ diffusion coefficient.

Table 8 Contribution of each diffusion compartment in the DWI signal according to the values of b (validation study)

b value (s/mm^2)	Global SI \pm SD	S1 ($f_1 \cdot e^{-b \cdot D_1}$)	S2 ($f_2 \cdot e^{-b \cdot D_2}$)	S3 ($f_3 \cdot e^{-b \cdot D_3}$)	(S2 + S3) / Global SI (%)	S3 / Global SI (%)
0	100.00	72.72	13.74	13.54	27.28	13.54
5	85.98 \pm 3.13	72.23	12.03	1.80	16.07	2.09
10	82.76 \pm 3.83	71.74	10.53	0.24	13.06	0.29
15	80.69 \pm 4.06	71.26	9.22	0.03	11.50	0.04
20	78.84 \pm 4.60	70.78	8.08	0.00	10.25	0.00
25	77.14 \pm 4.87	70.30	7.07	0.00	9.14	0.00
30	75.47 \pm 4.95	69.83	6.19	0.00	8.15	0.00
35	74.67 \pm 4.64	69.36	5.42	0.00	7.25	0.00
40	73.79 \pm 4.75	68.89	4.75	0.00	6.45	0.00
45	72.91 \pm 4.60	68.42	4.16	0.00	5.73	0.00
50	71.56 \pm 4.71	67.96	3.64	0.00	5.08	0.00
100	64.82 \pm 4.53	63.52	0.96	0.00	1.49	0.00
200	55.60 \pm 4.39	55.49	0.07	0.00	0.12	0.00
400	41.78 \pm 3.71	42.34	0.00	0.00	0.00	0.00
600	31.98 \pm 3.40	32.31	0.00	0.00	0.00	0.00
800	25.33 \pm 2.65	24.66	0.00	0.00	0.00	0.00

SI: Signal averaged and normalized for the 36 patients of the validation study

Si: Signal for diffusion compartment i

S2 + S3 / Global SI represents the contribution of perfusion in the global DWI signal

S3 / Global SI represents the contribution of compartment 3 in the global DWI signal

Due to limited sampling and the SNR of usual IVIM sequences, the study of the fastest compartment is probably unrealistic at an individual level. This third very fast (pseudo) diffusion component will be relevant for liver IVIM analysis when more sophisticated IVIM sequences become available.

Acknowledgements The scientific guarantor of this publication is Boris Guiu. The authors of this manuscript declare no relationships with any companies, whose products or services may be related to the subject matter of the article. The authors state that this work has not received any funding. One of the authors has significant statistical expertise. Institutional Review Board approval was obtained. Written informed consent was obtained from all subjects (patients) in this study. Methodology: prospective, observational, performed at one institution.

Appendix 1

¹H-MR Spectroscopy

¹H-MRS was performed in all patients. Semiautomated optimization of gradient shimming followed by manual adjustment of central frequency was performed, and water line widths of less than 25 Hz were obtained. Water suppression was not performed for any of the sequences.

Single-voxel MR spectroscopic data were acquired using seven breath-hold point-resolved spatially localized spectroscopic (PRESS) pulse sequences (repetition time, 5000 msec; three acquisitions; 2048 data points over 1250 Hz spectral width; and acquisition time, 15 sec) with echo times of 30, 40, 50, 60, 80, 100, and 135 msec to measure the T2 relaxation times of water and methylene (CH₂). A long TR was used to minimize T1 effects. Each breath-hold lasted 15 sec.

In all patients, the same 30*30*30-mm (27 ml) voxel was used for these seven sequences and was positioned obliquely on segment VII on the transverse low-T1-weighted section (thus avoiding extra-hepatic fat, large hepatic vessels, and organs adjacent to the liver).

¹H-MR spectroscopic data analysis

The Java-based MR user interface spectroscopic analysis package (jMRUI; A van den Boogaart, Catholic University, Leuven, Belgium) was used for the time-domain analysis. Metabolite signals were analyzed using the Advanced Magnetic Resonance (AMARES) fitting algorithm within jMRUI. We measured the water peak at 4.76 ppm and the methylene peak at 1.33 ppm. Spectra were used only if homogeneity after shimming, measured as the full width at 50 % peak height, was better than 25 Hz. Peak integrals were quantified by fitting to a Gaussian line shape.

T2 relaxation times of both metabolites were determined from their peak amplitudes at each echo time using an

exponential least-squares fitting algorithm. The peak areas of the methylene and water signals were then corrected for T2 effects (i.e., theoretical peak areas with 0 echo time), using the individually calculated T2 relaxation times.

LFC was calculated as follows:

$$\text{LFC}_{\text{MRS}} = 100 * A_{0\text{msec}_{\text{CH}_2}} / (A_{0\text{msec}_{\text{CH}_2}} + A_{0\text{msec}_{\text{WATER}}})$$

where $A_{0\text{msec}_{\text{CH}_2}}$ and $A_{0\text{msec}_{\text{WATER}}}$ were the areas of the methylene and water peaks, respectively, corrected for both T1 and T2 effects.

Triple-echo acquisition

A transverse breath-hold T1-weighted two-dimensional triple-echo spoiled gradient-echo sequence was performed through the liver with the following parameters: repetition time (msec)/echo time (msec) of 192/2.46 (in-phase [IP₁]), 3.69 (opposed-phase [OP]), and 4.92 (in-phase [IP₂]); flip angle, 60°; section thickness, 6 mm; intersection gap, 1.2 mm; matrix, 256*192; number of sections, 25; and acquisition time, 34 seconds. Parallel imaging (with an acceleration factor of 2) was performed using generalized autocalibrating partially parallel acquisition (GRAPPA; Siemens Medical Solutions Erlangen, Germany). Two separate breath-holds (each lasting 17 seconds) were needed to cover the entire liver volume.

Measurement of T2*

An ROI of 1–2 cm in diameter was drawn in the liver (avoiding large vessels, bile ducts or extra-hepatic areas) in five slices. The signal intensity (SI) in these five ROIs was averaged and recorded for IP1 (TE, 2.46 msec) and IP2 (TE, 4.92 msec) T1-weighted MR images. We used the copy-and-paste function of the workstation (Leonardo; Siemens Medical Solutions) to draw exactly the same ROIs at the same locations on IP images.

As previously reported [37, 38], the IP1 and IP2 images were used to estimate T2* relaxation time.

References

1. Guiu B, Cercueil JP (2011) Liver diffusion-weighted MR imaging: the tower of Babel? *Eur Radiol* 21:463–467
2. Guiu B, Petit JM, Capitan V et al (2012) Intravoxel incoherent motion diffusion-weighted imaging in nonalcoholic fatty liver disease: a 3.0-T MR study. *Radiology* 265:96–103
3. Le Bihan D (2008) Intravoxel incoherent motion perfusion MR imaging: a wake-up call. *Radiology* 249:748–752

4. Le Bihan D, Breton E, Lallemand D, Aubin ML, Vignaud J, Laval-Jeantet M (1988) Separation of diffusion and perfusion in intravoxel incoherent motion MR imaging. *Radiology* 168:497–505
5. Shah B, Anderson SW, Scalera J, Jara H, Soto JA (2011) Quantitative MR imaging: physical principles and sequence design in abdominal imaging. *Radiographics* 31:867–880
6. Clark CA, Le Bihan D (2000) Water diffusion compartmentation and anisotropy at high b values in the human brain. *Magn Reson Med* 44:852–859
7. Andreou A, Koh DM, Collins DJ et al (2013) Measurement reproducibility of perfusion fraction and pseudodiffusion coefficient derived by intravoxel incoherent motion diffusion-weighted MR imaging in normal liver and metastases. *Eur Radiol* 23:428–434
8. Delattre BM, Viallon M, Wei H et al (2012) In vivo cardiac diffusion-weighted magnetic resonance imaging: quantification of normal perfusion and diffusion coefficients with intravoxel incoherent motion imaging. *Invest Radiol* 47:662–670
9. Dijkstra H, Baron P, Kappert P, Oudkerk M, Sijens PE (2012) Effects of microperfusion in hepatic diffusion weighted imaging. *Eur Radiol* 22:891–899
10. Dyvorne HA, Galea N, Nevers T et al (2013) Diffusion-weighted imaging of the liver with multiple b values: effect of diffusion gradient polarity and breathing acquisition on image quality and intravoxel incoherent motion parameters—a pilot study. *Radiology* 266:920–929
11. Hayashi T, Miyati T, Takahashi J et al (2013) Diffusion analysis with triexponential function in liver cirrhosis. *J Magn Reson Imaging* 38:148–153
12. Lemke A, Stieltjes B, Schad LR, Laun FB (2011) Toward an optimal distribution of b values for intravoxel incoherent motion imaging. *Magn Reson Imaging* 29:766–776
13. Luciani A, Vignaud A, Cavet M et al (2008) Liver cirrhosis: intravoxel incoherent motion MR imaging—pilot study. *Radiology* 249:891–899
14. Pasquinelli F, Belli G, Mazzoni LN, Grazioli L, Colagrande S (2011) Magnetic resonance diffusion-weighted imaging: quantitative evaluation of age-related changes in healthy liver parenchyma. *Magn Reson Imaging* 29:805–812
15. Patel J, Sigmund EE, Rusinek H, Oei M, Babb JS, Taouli B (2010) Diagnosis of cirrhosis with intravoxel incoherent motion diffusion MRI and dynamic contrast-enhanced MRI alone and in combination: Preliminary experience. *J Magn Reson Imaging* 31:589–600
16. Ohtani O, Ohtani Y (2008) Lymph circulation in the liver. *Anat Rec (Hoboken)* 291:643–652
17. Moteki T, Horikoshi H (2011) Evaluation of noncirrhotic hepatic parenchyma with and without significant portal vein stenosis using diffusion-weighted echo-planar MR on the basis of multiple-perfusion-components theory. *Magn Reson Imaging* 29:64–73
18. Chandarana H, Taouli B (2010) Diffusion and perfusion imaging of the liver. *Eur J Radiol* 76:348–358
19. Lemke A, Laun FB, Simon D, Stieltjes B, Schad LR (2010) An in vivo verification of the intravoxel incoherent motion effect in diffusion-weighted imaging of the abdomen. *Magn Reson Med* 64:1580–1585
20. Guiu B, Loffroy R, Cercueil JP, Krause D (2008) Multiecho MR imaging and proton MR spectroscopy for liver fat quantification. *Radiology* 249:1081
21. Guiu B, Loffroy R, Petit JM et al (2009) Mapping of liver fat with triple-echo gradient echo imaging: validation against 3.0-T proton MR spectroscopy. *Eur Radiol* 19:1786–1793
22. Guiu B, Petit JM, Loffroy R et al (2009) Quantification of Liver Fat Content: Comparison of Triple-Echo Chemical Shift Gradient-Echo Imaging and in Vivo Proton MR Spectroscopy. *Radiology* 250:95–102
23. Jacqueminet S, Lebray P, Morra R et al (2008) Screening for liver fibrosis by using a noninvasive biomarker in patients with diabetes. *Clin Gastroenterol Hepatol* 6:828–831
24. Poynard T, Morra R, Halfon P et al (2007) Meta-analyses of FibroTest diagnostic value in chronic liver disease. *BMC Gastroenterol* 7:40
25. Ratzu V, Massard J, Charlotte F et al (2006) Diagnostic value of biochemical markers (FibroTest-FibroSURE) for the prediction of liver fibrosis in patients with non-alcoholic fatty liver disease. *BMC Gastroenterol* 6:6
26. Pekar J, Ligeti L, Ruttner Z et al (1991) In vivo measurement of cerebral oxygen consumption and blood flow using ¹⁷O magnetic resonance imaging. *Magn Reson Med* 21:313–319
27. Wirestam R, Brockstedt S, Lindgren A et al (1997) The perfusion fraction in volunteers and in patients with ischaemic stroke. *Acta Radiol* 38:961–964
28. Williams RL (2000) A note on robust variance estimation for cluster-correlated data. *Biometrics* 56:645–646
29. Motulsky H (2004) Fitting Models to Biological Data Using Linear and Nonlinear Regression : A Practical Guide to Curve Fitting
30. Anderson DR (2008) Model based inference in the life sciences: a primer on evidence.
31. Le Bihan D, Breton E, Lallemand D, Grenier P, Cabanis E, Laval-Jeantet M (1986) MR imaging of intravoxel incoherent motions: application to diffusion and perfusion in neurologic disorders. *Radiology* 161:401–407
32. Rani HP, Sheu TW, Chang TM, Liang PC (2006) Numerical investigation of non-Newtonian microcirculatory blood flow in hepatic lobule. *J Biomech* 39:551–563
33. Duong TQ, Kim SG (2000) In vivo MR measurements of regional arterial and venous blood volume fractions in intact rat brain. *Magn Reson Med* 43:393–402
34. Hayashi T, Miyati T, Takahashi J et al (2014) Diffusion analysis with triexponential function in hepatic steatosis. *Radiol Phys Technol* 7:89–94
35. Chow AM, Gao DS, Fan SJ et al (2012) Liver fibrosis: an intravoxel incoherent motion (IVIM) study. *J Magn Reson Imaging* 36:159–167
36. Colagrande S, Pasquinelli F, Mazzoni LN, Belli G, Virgili G (2010) MR-diffusion weighted imaging of healthy liver parenchyma: repeatability and reproducibility of apparent diffusion coefficient measurement. *J Magn Reson Imaging* 31:912–920
37. Guiu B, Petit JM, Loffroy R et al (2011) Liver methylene fraction by dual- and triple-echo gradient-echo imaging at 3.0 T: Correlation with proton MR spectroscopy and estimation of robustness after SPIO administration. *J Magn Reson Imaging* 33:119–127
38. Hussain HK, Chenevert TL, Londy FJ et al (2005) Hepatic fat fraction: MR imaging for quantitative measurement and display—early experience. *Radiology* 237:1048–1055